

Anodic Dissolution Behavior of the Crack Tip of X70 Pipeline Steel in Near-Neutral pH Environment

Zhongyu Cui, Liwei Wang, Zhiyong Liu, Cuiwei Du, Xiaogang Li, and Xin Wang

(Submitted May 24, 2016; in revised form September 19, 2016; published online October 21, 2016)

In this work, the anodic dissolution behavior of the fresh metal surface at crack tip of X70 steel in near-neutral pH environment was investigated using galvanic corrosion simulation method. The solution environment, strain, strain rate, hydrogen enrichment, and fresh metal surface at the crack tip were considered. Corrosion current of the specimen during fast stretching increased linearly with plastic strain. The increment and increase rate of the corrosion current during plastic deformation stage were dependent on the strain rate. Combining Faraday's law and crack tip strain rate equation, the crack growth rate (CGR) induced by the anodic dissolution of the fresh metal surface was calculated. Results show that CGR caused by anodic dissolution was roughly one order lower than that measured on the compact tensile specimen under cyclic load. This finding indicated that hydrogen embrittlement may play a dominate role in stress corrosion crack propagation of pipeline steels in near-neutral pH environment.

Keywords anodic dissolution, crack growth rate, crack tip, near-neutral pH, X70 pipeline steel

1. Introduction

Stress corrosion cracking (SCC) of steel in near-neutral pH environment has been a vital threat to the safe operation of buried oil/gas pipelines (Ref 1, 2). Although SCC behavior of pipelines has been extensively studied, quantifying the crack growth rate (CGR) during SCC is still difficult. The growth rate of stress corrosion cracks is related to the synergetic effect of hydrogen and stress on the anodic dissolution rate of fresh metal surface at the crack tip (Ref 3, 4). However, the direct *in situ* measurement of the rates of the important electrode processes, namely metal dissolution and reduction of water and hydrogen ions, is impractical. The kinetics can be quantified to a degree by conducting separate electrochemical experiments in conditions simulating that of the crack tip states, including the solution environment, mechanical levels, hydrogen content and fresh metal surface.

The mechanical and electrochemical states of the crack tip can be characterized using the following four aspects: solution environment, high strain and strain rate, high hydrogen concentration, and fresh metal surface (Ref 5-8). First, the solution near the crack tip is acidic because of the hydrolysis of Fe^{2+} and the occlusion effect. The generation of H^+ attracts Cl^-

to migrate to the crack tip area, resulting in a solution with low pH and high Cl^- concentration, which has been verified in our previous study, in which the solution pH and Cl^- concentration were identified as pH 4.0 and 3.8 mol/L (Ref 5), respectively. Secondly, during the crack propagation, a plastic deformation zone will form around the crack front, resulting in a high degree of strain and strain rate at the crack tip. Parkins et al. (Ref 6) noted that the strain rate of the crack tip could reach or even exceed 10^{-4} s^{-1} . Thirdly, an enrichment of hydrogen will occur around the crack tip because the stress level at the crack tip is high and the tensile stress can accelerate hydrogen invasion as well as increase hydrogen concentration. Qiao et al. (Ref 7) reported that the hydrogen concentration around the crack tip of pipeline steel in the acidified solution is approximately 7.0 ppm in weight. Finally, during crack propagation, fresh metal surface is produced at the crack tip. In this case, the electrochemical reaction around the crack tip is the polarization process of the fresh metal surface in the crack tip solution (Ref 9, 10).

The importance of the transient electrochemical reactions that proceed on freshly exposed metal surface at the crack tip has been emphasized because they are believed to control the crack growth in some material-environment systems (Ref 11-16). Beck et al. (Ref 11) and Alavi et al. (Ref 12) reviewed the techniques used to create fresh metal surfaces and separated them into five major groups as follows: forming liquid metal droplets, scraping or scratching a surface, straining a wire, shearing a wire, and rapid fracturing of a tensile specimen. A number of modifications have also been made based on these techniques in recent studies (Ref 13-16). Among them, the rapid fracturing of a tensile specimen has received attention particularly in the area of SCC. Zhao et al. (Ref 16) conducted simulation experiments using the rapid tensile test and obtained the contribution of anodic dissolution at the crack tip to the corrosion fatigue crack propagation rate for X80 steel in NaCl solution; however, the fresh metal surface and the enrichment of hydrogen at the crack tip in the simulation test were not considered. Therefore, a difference of at least three orders of magnitude between the measured CGR and the anodic dissolution-induced CGR was observed.

Zhongyu Cui, Corrosion and Protection Center, University of Science and Technology Beijing, Beijing 100083, China and Institute of Materials Science and Engineering, Ocean University of China, Qingdao 266100, China; **Liwei Wang**, College of Electromechanical Engineering, Qingdao University, Qingdao 266071, China; **Zhiyong Liu**, **Cuiwei Du**, and **Xiaogang Li**, Corrosion and Protection Center, University of Science and Technology Beijing, Beijing 100083, China; and **Xin Wang**, Institute of Materials Science and Engineering, Ocean University of China, Qingdao 266100, China. Contact e-mail: liuzhiyong7804@126.com.

To advance understanding of the SCC mechanism of pipeline steel in near-neutral pH environment, it is necessary to evaluate the electrochemical processes that occur at the crack tip more realistically. For this purpose, a galvanic corrosion simulation technique that facilitates the measurement of the electrochemical reactions at crack tip is proposed in this work. The corrosion current variation of the X70 specimen during straining is analyzed. The CGR induced by anodic dissolution of fresh metal surface at crack tip is calculated.

2. Experimental

2.1 Materials

The testing specimens were cut from a hot-rolling plate of API X70 pipeline steel with chemical composition (wt.%): 0.065 C, 1.57 Mn, 0.23 Si, 0.2 Ni, 0.18 Cr, 0.22 Cu, 0.056 Nb, 0.002 S, 0.0019 P, and Fe balance. The microstructure shown in Fig. 1 contained a ferrite matrix with a few small, dark martensite-austenitic particles at the grain boundaries. The yield strength of the material was 490 MPa, and its ultimate tensile strength was 610 MPa (determined under a strain rate of $1 \times 10^{-6} \text{ s}^{-1}$).

2.2 Electrochemical Measurement

Simulation experiments were carried out on a slow strain rate tensile test machine (WDML-30kN Materials Test System, Xi'an Lichuang, China) to determine the anodic dissolution of the crack tip. An electrochemical cell (Fig. 2a) was set up to simulate the mechanical and electrochemical states of the crack tip analyzed in the Introduction section. Traditional near-neutral pH solution (NS4) with a composition of 0.181 g/L $\text{CaCl}_2 \cdot 2\text{H}_2\text{O}$, 0.122 g/L KCl, 0.131 g/L $\text{MgSO}_4 \cdot 7\text{H}_2\text{O}$ and 0.483 g/L NaHCO_3 was acidified with acetic acid to obtain a pH of 4.0, and NaCl was added to obtain a Cl^- concentration of 0.4 mol/L. The solution chemistry was determined based on our previous work in which the pH and Cl^- concentration of the crack tip environment were identified as pH 4.0 and 3.8 mol/L by in situ measurements (Ref 5). Through the polarization curve testing, corrosion current density in solution with 0.4 mol/L of Cl^- is similar with that in a concentrated solution containing 4 mol/L of Cl^- . Therefore, the 0.4 mol/L was

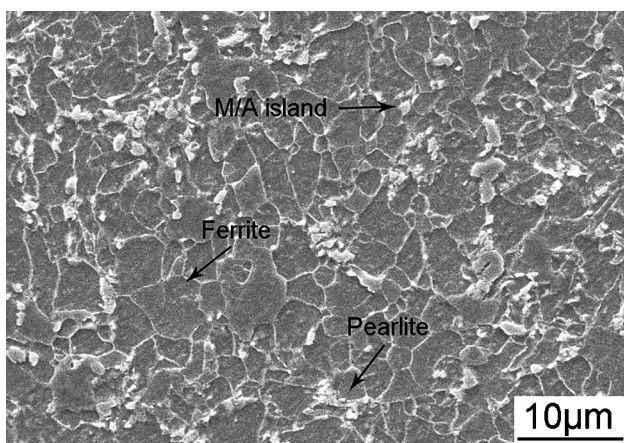


Fig. 1 Microstructure of X70 steel used in this work

chosen in this work. The solution was purged with N_2 gas for 4 h to achieve an anaerobic environment and the gas flow was maintained throughout the test. This solution was used to simulate the crack tip environment. The tensile specimen (work electrode, WE), which was fabricated according to GB/T 15970 (Ref 17), was used to simulate the crack tip area. The dimensions of the specimen are shown in Fig. 2(b), in which the samples were ground gradually to 2500 grit paper, rinsed with acetone and then covered with silicone rubber to leave an exposed area of 1.0 cm^2 . Before the electrochemical test, the specimen was charged in 0.2 mol/L NaOH + 0.25 g/L thiourea (H_2NCSNH_2) with a current density of 100 mA/cm^2 for 24 h. The hydrogen concentration was 7.1 ppm in weight measured using the hydrogen oxidization current method (Ref 18). For simplification, the crack tip and the crack walls are considered as the anode and cathode, respectively. As the crack tip area is much smaller than that of the crack walls, X70 steel with a dimension of $50 \text{ mm} \times 50 \text{ mm}$ was used as the counter electrode (CE) to simulate the crack walls. The galvanic corrosion module in Gamry Reference 3000 was used to measure the current between WE and CE. When the tensile specimen is stretched with a high strain rate, the mechanical state around the crack tip was simulated, and the strain-induced reduction of the electrode potential caused difference in potential between the WE and CE. Galvanic corrosion occurred afterward, and the tensile specimen served as anode and experienced dissolution. Meanwhile, the unloaded X70 specimen with a large area served as cathode to facilitate anodic dissolution. All the experiments were repeated three times to maintain the reproducibility, and all the tests were performed at ambient temperature (about $22 \text{ }^\circ\text{C}$).

2.3 Crack Growth Test

Compact tension (CT) specimens were used for the crack growth test of X70 pipeline steel which has been described in our previous work (Ref 19). The specimens were made in accordance with ASTM E647 (Ref 20), with the machined notch perpendicular to the rolling direction of the steel. The detailed sizes are shown in Fig. 3(a). The machined CT specimen was pre-cracked by fatigue in air to initiate a sharp crack tip from the machined notch. The crack lengths on both sides were controlled at 2.5 mm, and the total crack length from the loading line (including the notch) was typically 30.5 mm at the surface in this case. After pre-cracking, the specimen was cyclically loaded in the near-neutral pH solution. A triangle waveform was used with a loading frequency of 0.002 Hz and a stress ratio of 0.625. The maximum stress was controlled to achieve a maximum stress intensity factor (I_{max}) of $72.87 \text{ MPa m}^{0.5}$, and the stress intensity factor range (ΔK) was $27.3 \text{ MPa m}^{0.5}$. These values were calculated according to the following equation in ASTM E647 (Ref 20):

$$K = \frac{P}{BW^{1/2}} \cdot \frac{(2 + \alpha)\alpha^{1/2}}{(1 - \alpha)^{3/2}} \cdot [0.886 + 4.64\alpha - 13.32\alpha^2 + 14.72\alpha^3 - 5.6\alpha^4] \quad (\text{Eq 1})$$

where K is the stress intensity factor, P is the applied load, B is the thickness of the specimen, and W is the width of the specimen and the coefficient $\alpha = a/W$ (a is the crack length).

The crack length of the X70 pipeline steel in near-neutral pH environment was monitored through an *in situ* observation system (Fig. 3b), which has been used to investigate the crack

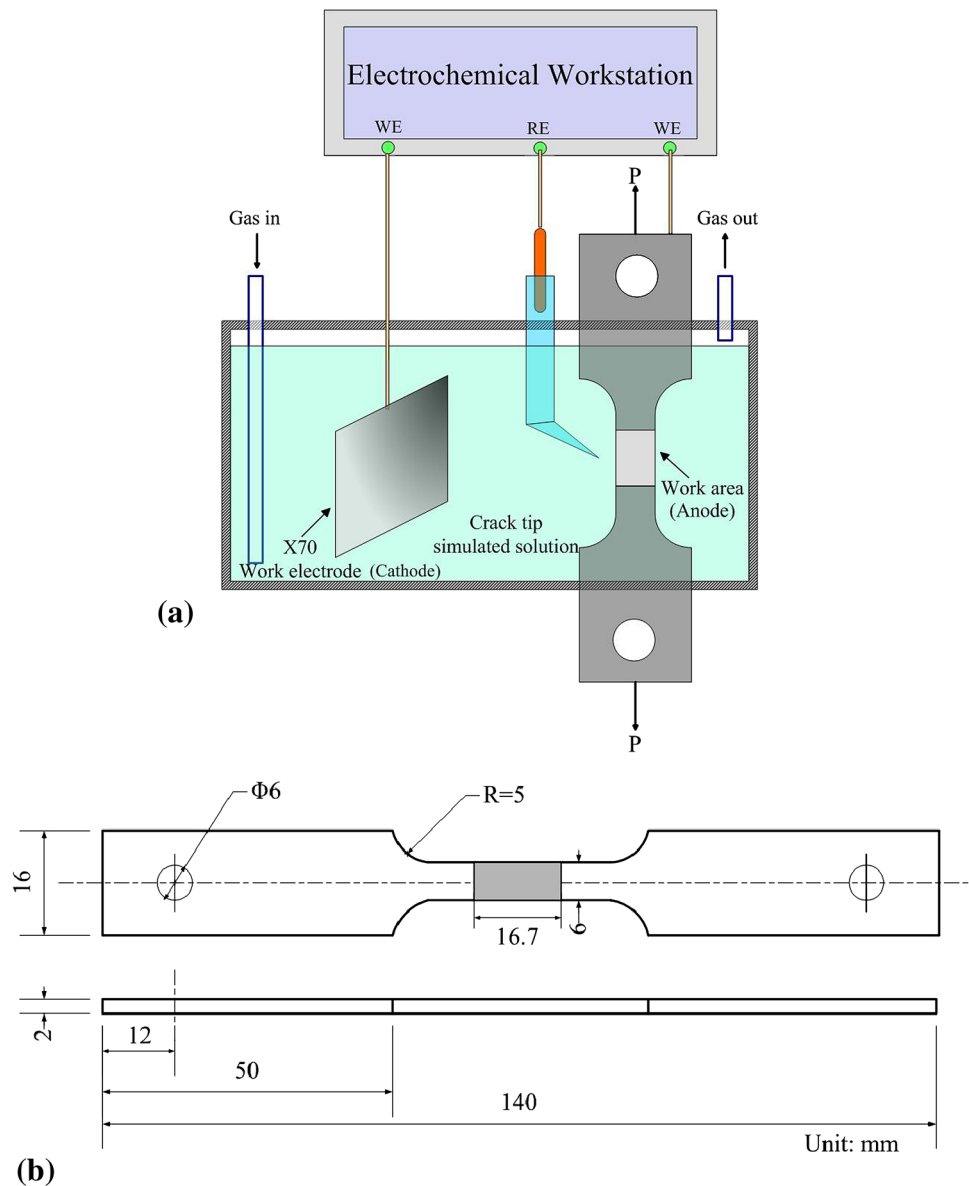


Fig. 2 Schematic diagram of the galvanic corrosion test to simulate the anodic dissolution of the crack tip (a) and geometry of the tensile specimen used in the electrochemical test

growth behavior in our previous studies (Ref 19, 21). The surface of the CT specimen during the crack growth test could be observed using a high-performance charge-coupled device (CCD) camera system. The head part of the CCD camera was mounted on an X-Z stage to monitor the crack tip. The system was operated using a computer, and reasonably clear images of the crack growth behavior could be obtained in the test.

3. Results

As described in section 2.2, the galvanic current density between the tensile specimen and the unloaded specimen are measured during the tensile test. Figure 4 illustrates the reproducibility of the galvanic current densities under a strain rate of $1 \times 10^{-4} \text{ s}^{-1}$. The variation tendencies of the three curves are very close and the mean values are used in the

following calculation. Three distinct regions are observed in the stress- t and i - t curves. In the elastic deformation region, the galvanic current fluctuates around a low value, indicating that galvanic corrosion is negligible. In the plastic deformation region, the galvanic current increases linearly with the tensile time (or strain) although some fluctuations also exist. After necking, the area of the specimen is visibly changed, and the galvanic current is not considered.

The galvanic current densities between the tensile specimen and the unloaded specimen under various strain rates are shown in Fig. 5. The corresponding stress- t curves are also shown in this figure. All of the i - t curves show similar shapes, with three distinct zones. The change in current density at the elastic deformation stage is negligible, but significantly increases at the plastic deformation stage. Moreover, under all strain rates, the current densities are proportional to the amount of the strain. Both the increment and the increase rate (i.e., the increase slope) of the galvanic current density during the plastic

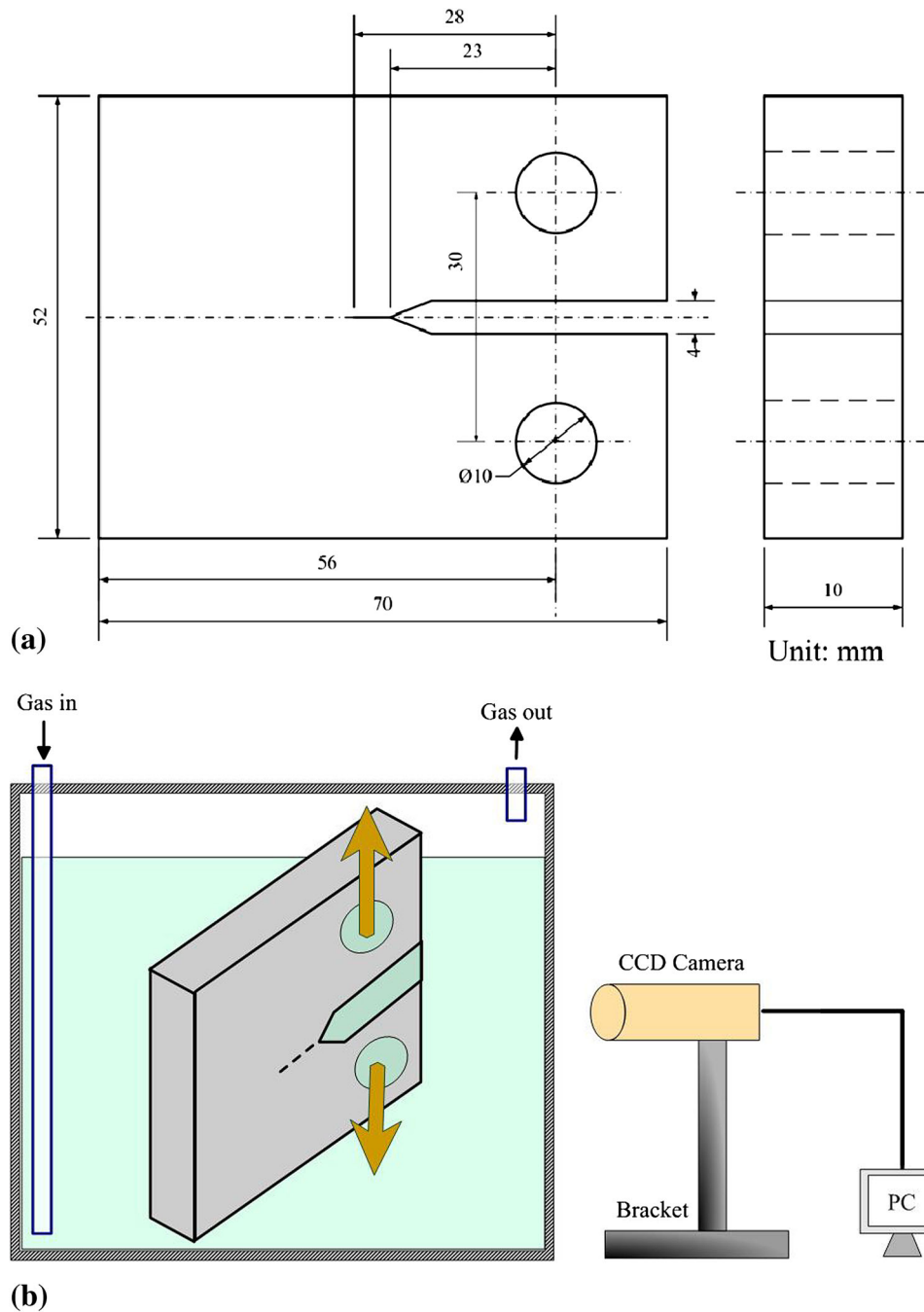


Fig. 3 Geometry of the compact tensile specimen (a) and the schematic diagram of crack length in situ measurement system (b)

deformation exhibit changes with the strain rates. Therefore, the two parameters are calculated based on these curves.

Figure 6 shows the increment and increase rate of the galvanic current during the plastic deformation. The increment in the current density induced by plastic deformation is calculated as the current density difference between the two dotted lines. Given that the galvanic current density increases linearly with the strain in the plastic deformation stage, the increase rate is calculated as the slope of the *i*-strain curve. Using this method, the calculated results are listed in Table 1 and shown in Fig. 7 and 8. It is shown that the increment in current density induced by the plastic deformation increases with the strain rate (Fig. 7). In addition, the slope of the *i*-strain curve increases linearly with the logarithm of strain rate

(Fig. 8). These results are in accordance with Hoar et al. (Ref 14) who reported that the rate of current increase was higher for higher strain rates.

Figure 9 shows the CGR in terms of da/dt as a function of ΔK . The CGR increases with the ΔK , with some fluctuations. The mean CGR during the crack propagation test is 8.56×10^{-5} mm/s.

4. Discussion

In general, galvanic corrosion will occur because of the potential difference between two metals in the presence of

corrosive medium. According to the mechanochemical model proposed by Gutman (Ref 22), the potential of metal will shift negatively when tensile stress is applied. Cheng et al. (Ref 23) pointed out that the potential drop of X70 steel in near-neutral pH environment is negligible in the elastic region, and this decrease becomes significant under plastic strain. Therefore, a potential difference exists between the loaded and unloaded specimen when the tensile test is started. The higher potential

difference in the plastic deformation region results in higher galvanic current density as shown in Fig. 4, 5 and 6.

Bockris et al. (Ref 24) suggested that the major factors affecting the anodic current of the specimens during straining were as follows: charging of the electric double layer on the fresh metal surface, increase in the surface roughness, emergence of the dislocation slip steps, and high index planes. They calculated the current increase induced by these factors and deduced the following equations:

$$\Delta i = k_1 \gamma i_e + k_2 \Delta E \dot{\epsilon} + (k_3 f i_{ns} + k_4 i_{hip}) \epsilon \dot{\epsilon} - k_5 i_{hip} \epsilon^2 \dot{\epsilon} \quad (\text{Eq 2})$$

where γ is the length of the dislocation slip steps, ΔE is the potential variation, f is the roughness coefficient, ϵ and $\dot{\epsilon}$ are the strain and strain rate, respectively. The $k_1 \sim k_5$ are constants, and i_e , i_{ns} , and i_{hip} are the current densities caused by slip steps, surface roughness and high index planes, respectively. This equation provides the probability to calculate the anodic current density cause by plastic strain, but the parameters in this equation are difficult to determine. Therefore, a simplified formula considering the anodic dissolution current of the crack tip is proposed according to the results that the current density increases linearly with the plastic strain:

$$i = i_0 + k_\epsilon \Delta \epsilon \quad (\text{Eq 3})$$

where i is the instantaneous galvanic current density, i_0 is the galvanic current density at the yield point, $\Delta \epsilon$ is the variation

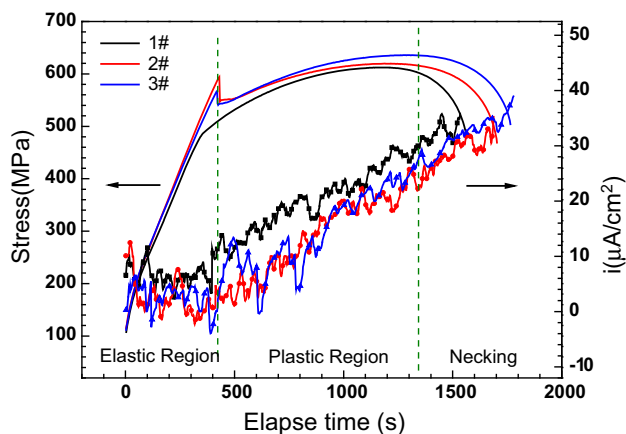


Fig. 4 Time dependence of the stress and current density flowing between deformed and non-deformed specimens of X70 steel

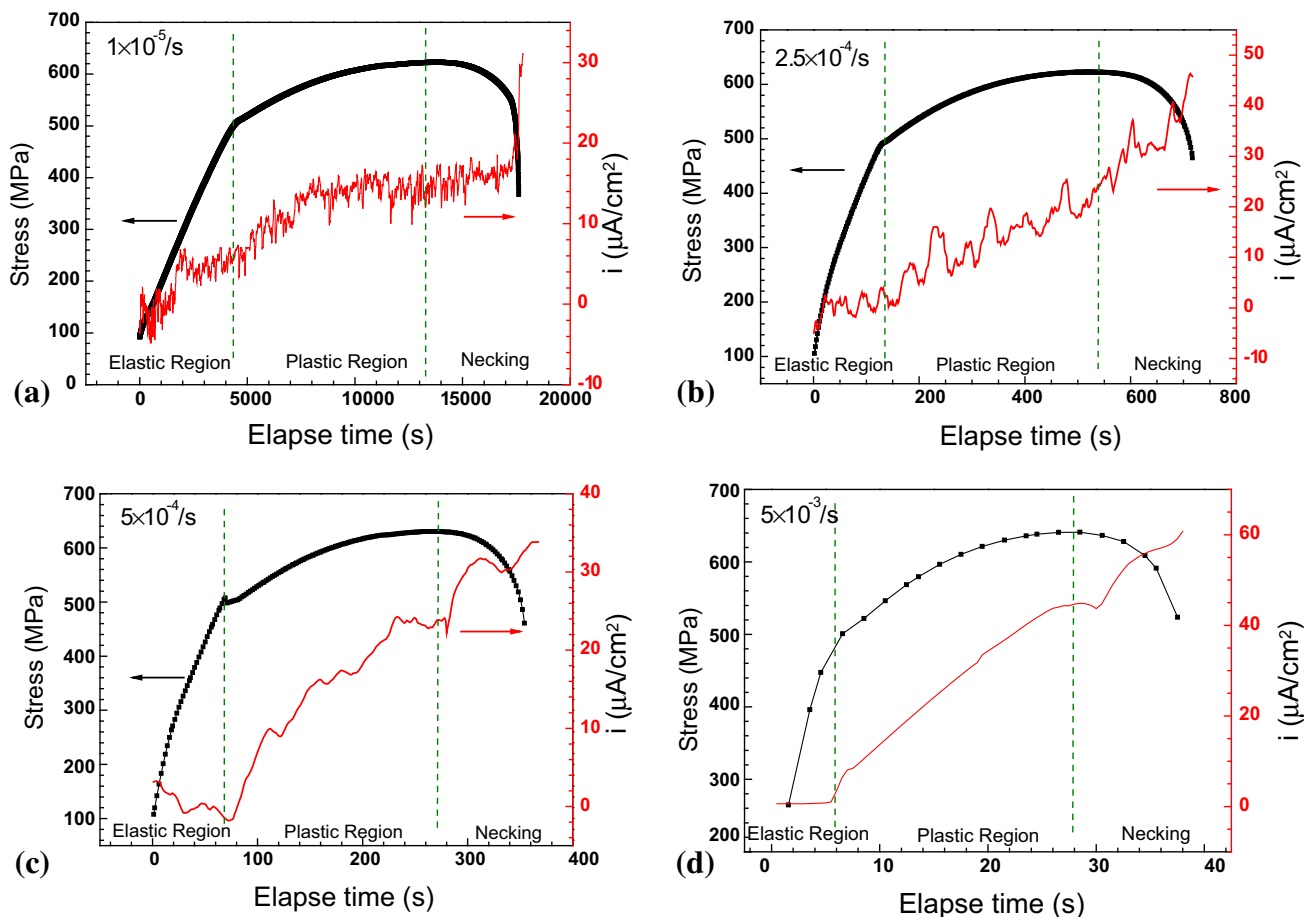


Fig. 5 Variations of the current densities during plastic deformation under different strain rates: (a) $1 \times 10^{-5} \text{ s}^{-1}$, (b) $2.5 \times 10^{-4} \text{ s}^{-1}$, (c) $5 \times 10^{-4} \text{ s}^{-1}$, (d) $5 \times 10^{-3} \text{ s}^{-1}$

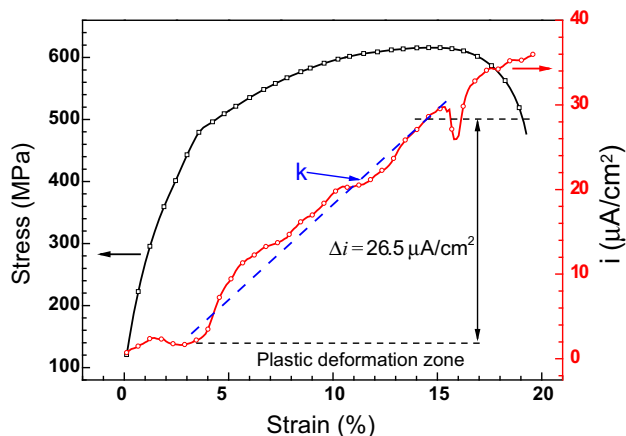


Fig. 6 Schematic diagram of the calculation method of the increments and increase rate (slope) of the current density during plastic deformation

Table 1 Increment and increase rate of the current density during plastic deformation under various strain rates

Strain rate, s ⁻¹	Increment in current density, μA/cm ²	Increase slope
1 × 10 ⁻⁵	12.46 ± 3.28	1.06 ± 0.28
5 × 10 ⁻⁵	17.73 ± 2.73	1.56 ± 0.24
1 × 10 ⁻⁴	20.92 ± 1.82	1.88 ± 0.15
2.5 × 10 ⁻⁴	22.91 ± 1.55	2.07 ± 0.11
5 × 10 ⁻⁴	25.72 ± 1.19	2.36 ± 0.16
1 × 10 ⁻³	28.37 ± 2.56	2.54 ± 0.22
5 × 10 ⁻³	43.90 ± 2.76	3.42 ± 0.25

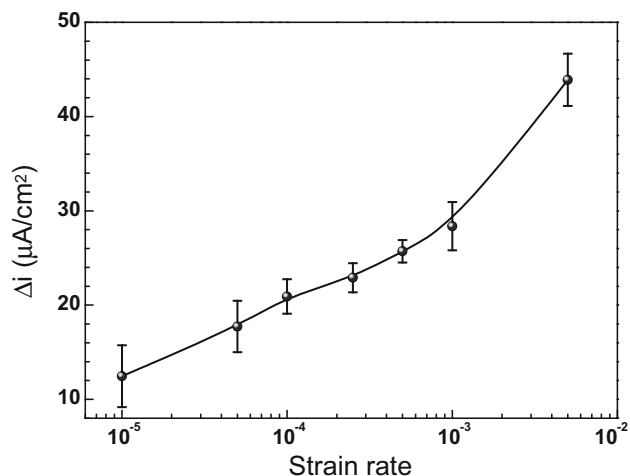


Fig. 7 Increment of the current density of X70 steel during plastic deformation under different strain rates

of plastic strain, and k is the increase slope that related to the strain rate. Gutman pointed out (Ref 22) that the mechanochemical effects in every dynamic plastic deformation were linearly dependent on deformation rate. Li et al. (Ref 25) also reported that a higher strain rate would significantly decrease the electron work function and thus enhance the electrochemical activity. In the present study, the increase

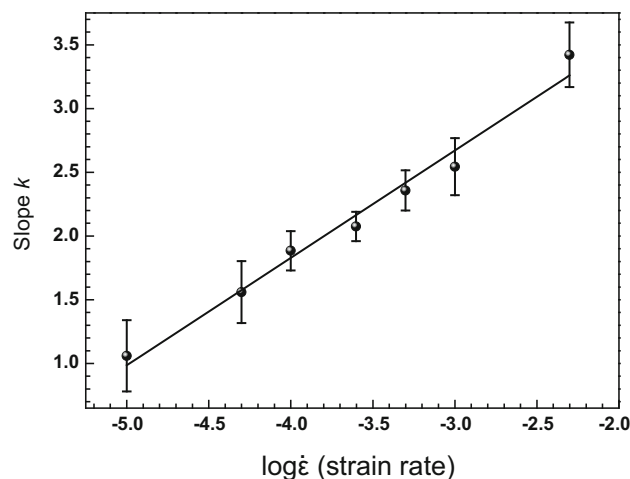


Fig. 8 Increase rate of the current density of X70 steel during plastic deformation under different strain rates

slope of the galvanic current increases linearly with the logarithm of the strain rates (Fig. 8) and it can be fitted as follows:

$$k_{\dot{\epsilon}} = 5.13 + \log \dot{\epsilon} \quad (\text{Eq 4})$$

Therefore, the instantaneous galvanic current density could be determined as follows:

$$i = i_0 + (5.13 + \log \dot{\epsilon}) \Delta \epsilon \quad (\text{Eq 5})$$

This equation can be used as the anodic current density of the crack tip during crack propagation.

Anodic dissolution (AD) and hydrogen embrittlement (HE) have been shown to be involved in the crack growth mechanism of pipeline steels in near-neutral pH environment (Ref 10, 26). Both of them contribute to the crack growth during the SCC process under cyclic load (Ref 27). In general, the crack growth rate of pipeline steels under cyclic load can be drawn as follows (Ref 28):

$$\begin{aligned} \left(\frac{da}{dt}\right)_{\text{total}} &= \left(\frac{da}{dt}\right)_{\text{fatigue}} + \left(\frac{da}{dt}\right)_{\text{SCC}} \\ &= C(\Delta K)^m + \left(\frac{da}{dt}\right)_{\text{AD}} + \left(\frac{da}{dt}\right)_{\text{HE}} \end{aligned} \quad (\text{Eq 6})$$

According to Faraday's law, CGR induced by AD can be obtained by (Ref 29)

$$\left(\frac{da}{dt}\right)_{\text{AD}} = i \frac{M}{zF\rho} = [i_0 + (5.13 + \log \dot{\epsilon}) \Delta \epsilon] \frac{M}{zF\rho} \quad (\text{Eq 7})$$

where M is the atomic weight of the metal (g/mol), i is corrosion current density (A/cm²), F is Faraday's constant (96,500 C/mol), z is the number of electrons exchanged during corrosion, and ρ is the density of the metal (g/cm³). In the present study, i_0 is negligible because the potential variation during the elastic deformation is small. $\Delta \epsilon$ is identified as 10% which is a high uniform plastic strain around the crack tip. In this case, the crack propagation induced by anodic dissolution can be determined when the strain rate at the crack tip during the cyclic load is obtained.

The crack tip strain rate during crack propagation under cyclic load has been reported by many researchers (Ref 16,

30-33). According to Shoji et al. (Ref 30, 31) and Lu et al. (Ref 32, 33), the strain rate at the tip of the propagating crack under cyclic loading can be calculated from the following formula:

$$\dot{\varepsilon} = \dot{\varepsilon}_K + \dot{\varepsilon}_{\dot{a}} = f d_n \frac{\Delta K^2}{E \sigma_y} + \frac{N^*}{N^* - 1} \frac{\dot{a}}{r_0} \frac{\beta \sigma_y}{E} \times \left\{ \ln \left[\frac{(1+R)^2 \Delta K^2}{4 \cdot (1-R)^2 3\pi r_0 \sigma_y^2} \right] \right\}^{\frac{1}{N^*-1}} \quad (\text{Eq 8})$$

The physical meanings and the corresponding values of the parameters used in this equation are listed in Table 2. The strain rates at the crack tip can be calculated using the instant crack growth velocity (\dot{a}) and ΔK values from the test results in Fig. 9. Then, the CGR induced by AD is calculated and shown in Fig. 10 as compared with the measured crack propagation rate. It is seen that the CGR caused by AD is much smaller than the total CGR. Therefore, other aspects should be considered to provide more reliable results. In the above calculations, the current density increments are supposedly equivalent to the anodic dissolution current induced by uniform plastic deformation (Ref 16). However, the AD current of the fresh metal surface, which really controls the AD-induced crack propagation, is disregarded. The anodic current of the fresh metal surface during straining should be calculated.

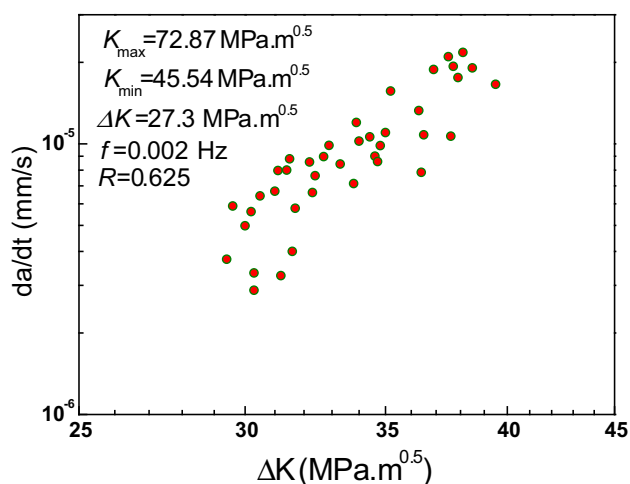


Fig. 9 Crack growth rate of X70 steel in near-neutral pH environment in terms of da/dt as a function of ΔK

Assuming that the newly generated fresh surface area is ΔS at a certain plastic strain, the relationship among the ΔS , the original surface area (S_0), and the gauge length (L_0) follows the equation below proposed by Bubar et al. (Ref 34):

$$\frac{\Delta S}{S_0} = 1 - \left(\frac{L_0}{L} \right)^{\frac{1}{2}} \quad (\text{Eq 9})$$

where L is the gauge length after plastic strain. Assuming that the corrosion current densities of the specimen before and after plastic strain are i_0 and i_p , respectively, and the corrosion current density of the fresh metal surface is i_f , then the following equation is satisfied approximately:

$$S_0 i_0 + \Delta S i_f = S_0 i_p \quad (\text{Eq 10})$$

Then, the corrosion current of the fresh metal surface can be calculated:

$$i_f = \frac{S_0 (i_p - i_0)}{\Delta S} = \frac{i_p - i_0}{1 - \left(\frac{L_0}{L} \right)^{\frac{1}{2}}} \quad (\text{Eq 11})$$

During plastic deformation, the relationship between the strain value and the gauge length follows the formula:

$$\varepsilon = \frac{L - L_0}{L_0}, \quad \text{and} \quad \frac{L_0}{L} = \frac{1}{1 + \varepsilon} \quad (\text{Eq 12})$$

Equation 12 is then factored into Eq 11 and the corrosion current of the fresh metal surface during plastic strain is obtained as follows:

$$i_f = \frac{\Delta i}{1 - \left(\frac{1}{1 + \varepsilon} \right)^{\frac{1}{2}}} \quad (\text{Eq 13})$$

where Δi is the corrosion current variation due to the plastic strain. By combining Eq 7, 8, and 13, the CGR induced by AD of the fresh metal surface at the crack tip can be calculated, and the results are also shown in Fig. 10. The CGR induced by the AD of the fresh metal surface is about 2.5×10^{-7} mm/s, which is one order greater than that calculated using the corrosion current of the whole surface. However, a difference of at least one order of magnitude between the measured CGR and the AD-induced CGR is observed, which is mainly attributed to several reasons. Firstly, the loading frequency used in this work is 0.002 Hz, which is a very low frequency for the mechanical fatigue. Therefore, the CGR caused by the pure mechanical fatigue could be

Table 2 Physical meanings and the corresponding values of the parameters used in the formula of the crack tip strain rate

Parameters	Description	Values
\dot{a} (m/s)	Instant crack growth velocity	Measured data
r_0 (m)	Specific length for crack tip strain rate calculation for steel	1×10^{-6} to 5×10^{-6} (Ref 31)
N^*	Strain hardening exponent	1.6 (Ref 32)
β	Rice coefficient	5.08 (Ref 33)
d_n	Constant depending on the stress state and the strain hardening exponent	0.3 (Ref 16)
σ_y (MPa)	Yield strength	X70 (450 MPa)
E (GPa)	Young's modulus for pipeline steel	206
R	Stress ratio	0.625
K_{\max} (MPa ^{1/2})	Maximum stress intensity factor	72.87
ΔK (MPa ^{1/2})	Stress intensity factor range	27.3
f (HZ)	Frequency	0.002

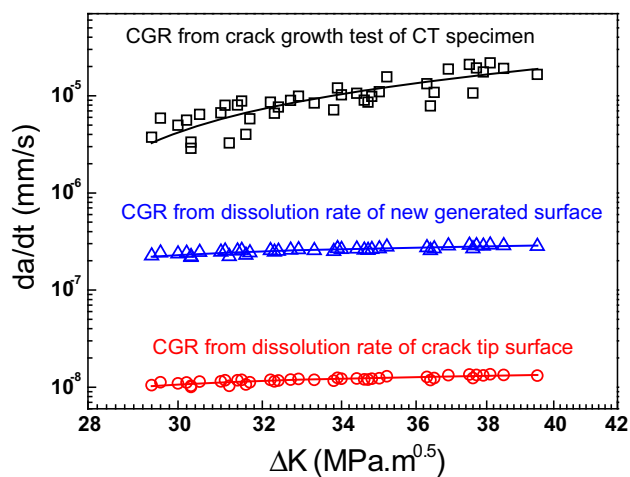


Fig. 10 Comparison of the crack growth rate of X70 steel between the measured results on CT specimen and the calculated results from the anodic dissolution

ignored. The second aspect that affects the stress corrosion cracking is the HE effect. During the SCC process of pipeline steel in near-neutral pH environment, the hydrogen will migrate to the crack tip area and produce enrichment around the crack tip. The accumulated hydrogen atoms not only facilitate the AD but also accelerate the HE, resulting in a high crack growth rate. Therefore, in this work, the higher measured CGR on the CT specimen is mainly attributed to the hydrogen-induced cracking.

5. Conclusions

The anodic dissolution at the crack tip of X70 steel during SCC was investigated using a simulation technique. The main conclusions can be drawn as follows:

- (1) The mechanical and electrochemical states at the crack tip can be simulated using the well-controlled galvanic corrosion method.
- (2) Corrosion current of the specimen during fast stretching increases linearly with the plastic strain.
- (3) The increment of the corrosion current and the increase rate during the plastic deformation stage is related to the strain rate. An empirical formula between the corrosion current and the plastic strain and strain rate is obtained.
- (4) CGR induced by AD of the fresh metal surface at the crack tip is calculated based on Faraday's law and crack tip strain rate. The value is roughly one order smaller than the measured CGR during cyclic load.
- (5) Hydrogen embrittlement may play a dominate role in stress corrosion crack propagation of pipeline steels in near-neutral pH environment.

Acknowledgments

The authors wish to acknowledge the financial support of National Natural Science Foundation of China (Nos. 51471034,

51131001 and 51601182) and National Basic Research Program of China (973 Program Project, No. 2014CB643300).

References

1. R.N. Parkins, W. Blanchard, Jr., and B. Delanty, Transgranular Stress Corrosion Cracking of High-Pressure Pipelines in Contact with Solutions of Near Neutral pH, *Corrosion*, 1994, **50**, p 394–408
2. J.A. Beavers, 2013 Frank Newman Speller Award Lecture: Integrity Management of Natural Gas and Petroleum Pipelines Subject to Stress Corrosion Cracking, *Corrosion*, 2013, **70**, p 3–18
3. X. Tang and Y.F. Cheng, Quantitative Characterization by Micro-Electrochemical Measurements of the Synergism of Hydrogen, Stress and Dissolution on Near-Neutral pH Stress Corrosion Cracking of Pipelines, *Corros. Sci.*, 2011, **53**, p 2927–2933
4. Y. Huang, F.Z. Xuan, S.T. Tu, and T. Itoh, Effects of Hydrogen and Surface Dislocation on Active Dissolution of Deformed 304 Austenitic Stainless Steel in Acid Chloride Solution, *Mater. Sci. Eng. A*, 2011, **528**, p 1882–1888
5. Z.Y. Cui, Z.Y. Liu, X.Z. Wang, Q. Li, C.W. Du, and X.G. Li, Crack Growth Behavior and Crack Tip Chemistry of X70 Pipeline Steel in Near-Neutral pH Environment, *Corros. Eng. Sci. Technol.*, 2016, **51**, p 352–357
6. R.N. Parkins, Current Topics in Corrosion: Factors Influencing Stress Corrosion Crack Growth Kinetics, *Corrosion*, 1987, **43**, p 130–139
7. L.J. Qiao, J.L. Luo, and X.J. Mao, Hydrogen Evolution and Enrichment Around Stress Corrosion Crack Tips of Pipeline Steels in Dilute Bicarbonate Solution, *Corrosion*, 1998, **54**, p 115–120
8. Z.Y. Liu, X.G. Li, and Y.F. Cheng, Effect of Strain Rate on Cathodic Reaction During Stress Corrosion Cracking of X70 Pipeline Steel in a Near-Neutral pH Solution, *J. Mater. Eng. Perform.*, 2011, **20**, p 1242–1246
9. R.N. Parkins, Predictive Approaches to Stress Corrosion Cracking Failure, *Corros. Sci.*, 1980, **20**, p 147–166
10. Z.Y. Liu, X.G. Li, and Y.F. Cheng, Mechanistic Aspect of Near-Neutral pH Stress Corrosion Cracking of Pipelines Under Cathodic Polarization, *Corros. Sci.*, 2012, **55**, p 54–60
11. T.R. Beck, Electrochemical Techniques for Corrosion: Symposium on Electrochemical Techniques for Corrosion at the NACE Corrosion/76 meeting held in Houston, Texas, March 22–26, 1976, NACE1977
12. A. Alavi, C.D. Miller, and R.P. Wei, A Technique for Measuring Kinetics of Electrochemical Reactions with Bare Metal Surfaces, *Corrosion*, 1987, **43**, p 204–207
13. R.P. Wei, M. Gao, and P.Y. Xu, Peak Bare Surface Current Densities Overestimated in Straining and Scratching Electrode Experiments, *J. Electrochem. Soc.*, 1989, **136**, p 1835–1836
14. T.P. Hoar and J.R. Galvele, Anodic Behaviour of Mild Steel During Yielding in Nitrate Solutions, *Corros. Sci.*, 1970, **10**, p 211–224
15. R.C. Newman and K. Sieradzki, Electrochemical Aspects of Stress-Corrosion Cracking of Sensitized Stainless Steels, *Corros. Sci.*, 1983, **23**, p 363–378
16. W. Zhao, R. Xin, Z. He, and Y. Wang, Contribution of Anodic Dissolution to the Corrosion Fatigue Crack Propagation of X80 Steel in 3.5 wt.% NaCl Solution, *Corros. Sci.*, 2012, **63**, p 387–392
17. GB-T15970, Chinese National Standard for Stress Corrosion Cracking Tests, 2007
18. J. Capelle, I. Dmytrakh, and G. Pluvinaige, Comparative Assessment of Electrochemical Hydrogen Absorption by Pipeline Steels with Different Strength, *Corros. Sci.*, 2010, **52**, p 1554–1559
19. Z.Y. Cui, Z.Y. Liu, L.W. Wang, C.W. Du, and X.G. Li, Effect of pH Value on the Crack Growth Behavior of X70 Pipeline Steel in the Dilute Bicarbonate Solutions, *Mater. Trans.*, 2015, **56**, p 777–780
20. ASTM E647, Standard test method for fatigue crack growth rates, *The American Society for Testing of Materials*, 2005
21. M. Zhu, G. Ou, H. Jin, C. Du, X. Li, and Z. Liu, Study on the Crack Propagation Behavior of X80 Pipeline Steel Under AC Application in High pH Solution, *J. Mater. Eng. Perform.*, 2015, **24**, p 2422–2425
22. E.M. Gutman, *Mechanochemistry of Materials*, Cambridge Int Science Publishing, Cambridge, 1998
23. L.Y. Xu and Y.F. Cheng, Corrosion of X100 Pipeline Steel Under Plastic Strain in a Neutral pH Bicarbonate Solution, *Corros. Sci.*, 2012, **64**, p 145–152

24. A.R. Despic, R.G. Raicheff, and J.O.M. Bockris, Mechanism of the Acceleration of the Electrode Dissolution of Metals During Yielding Under Stress, *J. Chem. Phys.*, 1968, **49**, p 926–938
25. W. Li, M. Cai, Y. Wang, and S. Yu, Influences of Tensile Strain and Strain Rate on the Electron Work Function of Metals and Alloys, *Scripta Mater.*, 2006, **54**, p 921–924
26. Z.Y. Cui, Z.Y. Liu, L.W. Wang, H.C. Ma, C.W. Du, X.G. Li, and X. Wang, Effect of pH Value on the Electrochemical and Stress Corrosion Cracking Behavior of X70 Pipeline Steel in the Dilute Bicarbonate Solutions, *J. Mater. Eng. Perform.*, 2015, **24**, p 4400–4408
27. B.T. Lu, Crack Growth Model for Pipeline Steels Exposed to Near-Neutral pH Groundwater, *Fatigue Fract. Eng. Mater. Struct.*, 2013, **36**, p 660–669
28. W. Chen and R.L. Sutherby, Crack Growth Behavior of Pipeline Steel in Near-Neutral pH Soil Environments, *Metall. Mater. Trans. A*, 2007, **38**, p 1260–1268
29. F.M. Song, Predicting the Mechanisms and Crack Growth Rates of Pipelines Undergoing Stress Corrosion Cracking at High pH, *Corros. Sci.*, 2009, **51**, p 2657–2674
30. T. Shoji, Z. Lu, and H. Murakami, Formulating Stress Corrosion Cracking Growth Rates by Combination of Crack Tip Mechanics and Crack Tip Oxidation Kinetics, *Corros. Sci.*, 2010, **52**, p 769–779
31. Q.J. Peng, J. Kwon, and T. Shoji, Development of a Fundamental Crack Tip Strain Rate Equation and Its Application to Quantitative Prediction of Stress Corrosion Cracking of Stainless Steels in High Temperature Oxygenated Water, *J. Nucl. Mater.*, 2004, **324**, p 52–61
32. B.T. Lu, F. Song, M. Gao, and M. Elboudjaini, Crack Growth Model for Pipelines Exposed to Concentrated Carbonate–Bicarbonate Solution with High pH, *Corros. Sci.*, 2010, **52**, p 4064–4072
33. B.T. Lu, Further Study on Crack Growth Model of Buried Pipelines Exposed to Concentrated Carbonate–Bicarbonate Solution, *Eng. Fract. Mech.*, 2014, **131**, p 296–314
34. S.F. Bubar and D.A. Vermilyea, Deformation of Anodic Oxide Films, *J. Electrochem. Soc.*, 1966, **113**, p 892–895